Peer-reviewed version available at *Vision* **2019**, *3*, 5; doi:10.3390/vision3010005

Temporal limits of visual motion processing: psychophysics and neurophysiology

Bart G. Borghuis[1,5,*], Duje Tadin[2,4], Martin J.M. Lankheet[3,5], Joseph S. Lappin[4,5], Wim A. van de Grind[5]

[1]Department Anatomical Sciences and Neurobiology, University of Louisville School of Medicine, Louisville, KY, USA.
[2]Brain and Cognitive Sciences, Center for Visual Science, Neuroscience, and Ophthalmology; University of Rochester, Rochester, NY, USA
[3]Department of Animal Sciences, Wageningen University, Wageningen, Gelderland, The Netherlands
[4]Vanderbilt Vision Research Center, Vanderbilt University, Nashville, TN, USA
[5]Helmholtz Institute and Department of Functional Neurobiology, Utrecht University, Utrecht, The Netherlands

[*]Corresponding author: bart.borghuis@louisville.edu.

Abstract: Under optimal conditions, just 3-6 ms of visual stimulation suffices for humans to see motion. Motion perception on this time scale implies that the visual system under these conditions reliably encodes, transmits, and processes neural signals with near-millisecond precision. Motivated by *in vitro* evidence for high temporal precision of motion signals in the primate retina, we investigated how neuronal and perceptual limits of motion encoding relate. Specifically, we examined the correspondence between the time scale at which cat retinal ganglion cells *in vivo* represent motion information and temporal thresholds for human motion discrimination. The time scale for motion encoding by ganglion cells ranged from 4.6-91 ms, depended nonlinearly on temporal frequency but not on contrast. Human psychophysics revealed that minimal stimulus durations required for perceiving motion direction were similarly brief, 5.6-65 ms, similarly depended on temporal frequency but, above ~10%, not on contrast. Notably, physiological and psychophysical measurements corresponded closely throughout (r = 0.99), despite more than a 20-fold variation in both human thresholds and optimal time scales for motion encoding in the retina. These results demonstrate that neural circuits for motion vision in cortex can maintain and make use of the high temporal fidelity of the retinal output signals.

Keywords: human psychophysics; apparent motion; temporal integration; cat; retina; neural coding; Hassenstein-Reichardt detector; model analysis

1. Introduction

It has been long known that the mammalian visual system is highly sensitive to motion, even when presented briefly. For example, Exner [1] reported that when humans view two sequentially flashed stimuli, the threshold for temporal order detection could be as short as 15 ms. Subsequent studies showed that under optimal conditions even 3 - 6 ms temporal-order asynchrony can be reliably discriminated [2-4]. Under these circumstances, the two stimuli are not perceived separately but as a single moving object ('apparent motion'), indicating that the percept involves visual motion processing.

The middle temporal visual area (area MT, or V5) is a region of extrastriate visual cortex in primates that has been demonstrated to be critical for motion vision [5]. Area MT has among the shortest response latencies in extrastriate cortex [6], consistent with the observation that human reaction times are shorter for moving compared with stationary objects [7]. A short response latency is functionally meaningful because it enables a rapid response to stimulus onset, for example, during collision avoidance. But appropriate behavioral responses in a dynamic visual environment also require information about the stimulus – such as the direction of motion – to be resolved at a high temporal rate [8]. Thus, there is a benefit to encoding stimulus information on the briefest possible time scale.

Visual encoding starts in the retina, where visual transduction and signal processing within retinal neural circuits culminates in selective encoding of the visual input by the ganglion cells. Ganglion cells transmit visual information as series of action potentials (spike trains) through the optic nerve, via the lateral geniculate nucleus (LGN) of the thalamus, to the visual cortex. The majority of ganglion cells in the retina of cats and primates signal spatio-temporal changes in luminance contrast but do not, by themselves, provide information about motion direction. Instead, current working models suggest that motion vision depends on the integration of signals from multiple ganglion cells with spatially offset visual receptive fields [9-12]. This is supported by computational analysis of population macaque retinal parasol-type ganglion cell responses to a moving bar recorded *in vitro*, which showed that motion direction could be reconstructed from temporal correlations in the cells' spike trains at a time scale of 10–50 ms [13, 14]. Thus, the time scale at which ganglion cell spike train ensembles represent visual motion approaches the inter-spike interval. This suggests that noise variations (variability) in neuronal spike timing may limit the temporal fidelity of visual motion encoding [15, 16], but to what extent they do so has remained unclear.

Variability in neuronal spike timing is apparent from trial-to-trial variations in the times at which a cell fires action potentials in response to repeated presentations of the same stimulus. Spike timing variability stems from noise in neuronal signal transduction and transmission, and its demonstrated underlying sources include quantal fluctuations in photon absorption, fluctuations in cyclic nucleotides within the photoreceptors, as well as noise in ion channels and synaptic vesicle release [17]. For several of these factors, the noise amplitude depends on stimulus parameters such as stimulus temporal frequency and luminance contrast [18-21]. Here, we postulate that if spike timing variability limits the encoding of visual motion information, then the time scale for resolving visual motion at the perceptual level should similarly depend on these stimulus parameters. In agreement with this idea, model analysis of retinal ganglion cells responses obtained from primate retina *in vitro* showed that the optimal time scale for decoding retinal motion signals decreases with temporal frequency and contrast [13]. While other studies have explored the relation between encoding accuracy at the neuronal and behavioral level for chromatic [22] and orientation discrimination tasks [23], how the time scale of population motion encoding in the retina relates to the temporal limits of visual motion perception remains unclear.

To address this, we assessed the relation between the time scale of motion encoding in mammalian retinal ganglion cells *in vivo* and the temporal limits of human motion perception. We first recorded cat X- and Y-type ganglion cell spike responses to motion stimuli with a range of contrasts and temporal frequencies. We then used model analysis to compute from these responses, for each stimulus condition, the time scale at which they best represent motion information. The measured time scales approximated those reported for macaque parasol cells, supporting the assumption that the temporal precision of the retinal spike output for a subset of ganglion cell types is similar across mammals. We then measured for matched stimuli in humans the minimum stimulus duration required for motion direction discrimination.

We found that across stimuli, the temporal limit for visual motion discrimination at the perceptual level closely matched the time scale of motion encoding at the ganglion cell level. Thus, it appears that human motion perception adheres to the temporal fidelity of visual encoding at the level of the retinal ganglion cells. Based on these results we conclude that the visual cortex both maintains and makes use of the stimulus-dependent temporal fidelity of the retinal output for resolving visual motion.

2. Results

2.1 Electrophysiology and modeling

We recorded extracellular spike responses to repeated presentations of drifting sine wave gratings from 37 retinal ganglion cells (n = 33 X type, 4 Y type) from the optic tract and 20 visual relay cells (all X type) from the lateral geniculate nucleus of anesthetized cats *in vivo*. Spatial frequency was optimized for each cell, and temporal frequency and luminance contrast were varied (0.5 – 16 Hz; 10 - 70%). Increasing contrast increased the modulation amplitude of a cell's firing rate, as expected (Figure 1). We used the recorded spike trains as input to a motion detector model to determine the time scale at which their temporal structure represented motion information (see Methods for details).

The motion detector was modeled as a correlator in which input spike trains were first low-pass filtered with a leaky integrator-type filter characterized by a time constant τ (Figure 2A) and then integrated. This choice of filter was motivated by its simplicity and physiological relevance, as for a range of values of τ the exponential tail can be interpreted as a first-order description of a receiving neuron's postsynaptic potential [24]. Low-pass filtering transformed the spike train from a temporal point process with time-varying rate into a continuous signal – a series of superimposed pulses with exponentially decaying tails.

Due to variability in spike timing, spikes in the two input spike trains rarely occurred within the same 0.5 ms spike acquisition time bin. Thus, for very small values of τ (<1 ms), cross-multiplication of the two spike trains gave a near-zero output signal (Figure 2B). For large values of τ, on the other hand, the correlator was largely insensitive to the timing of individual spikes, and its output reflected the mean difference in firing rate [24], which was normalized in the model, so that for large τ, signal correlation approached unity. Between these two extremes, correlation grew monotonically with the value of the time constant (Figure 3).

To determine how much motion information was carried by the temporal structure of the spike trains, the procedure was repeated after randomly shuffling the inter-spike intervals in each spike train. This eliminated temporal structure while preserving response statistics such as mean firing rate and the inter-spike interval histogram. Again, correlation as a function of τ was a monotonic function (Figure 3). However, shuffling shifted the curve towards larger τ, indicating that to obtain the same level of correlation now required a longer integration time.

The shift shows that by discarding the temporal structure of the spike trains, motion information was lost. Exactly how much information was lost is expressed by the difference between the original curve and the shuffled response curve (Figure 3). This difference function peaked at an intermediate value of τ, about 23 ms in this example. At this integration time, the motion detector maximally extracts motion information from the temporal structure of the input spike trains. We defined this value of τ as the optimal integration time (τ_{opt}).

While temporal correlation between spike responses increased with increasing stimulus contrast, above about 10%, contrast had very little effect on the optimal integration time (Figure 4). This was surprising, considering the large apparent effect of contrast on spike timing variability (Figure 1). Instead, optimal integration times depended strongly on temporal frequency: increasing temporal frequency caused correlation curves to peak at shorter integration times. This effect was robust (~20-fold change across presented frequency range) and was observed for all recorded cell types (retinal X, Y and LGN X-cells; Figure 5).

Retinal Y cells had the shortest optimal integration time, ranging from 79 ms at 0.5 Hz to 4.6 ms at 16 Hz (n = 4), indicating that these cells had the highest temporal fidelity. The optimal integration time for retinal X cells was slightly longer, ranging from 91 ms at 0.5 Hz to 6.6 ms at 16 Hz (n = 33). The optimal integration time for LGN X cells was slightly longer again, ranging from 113 ms at 0.5 Hz to 7.3 ms at 16 Hz. Optimal integration times for LGN X cell responses were on average 26.3 ± 13 % longer than those for retinal X cells, suggesting some loss of temporal precision at the LGN-relay. Optimal integration times for Y type retinal ganglion cells were on average 18.4 ± 7.8 ms shorter than for retinal X cell responses, demonstrating greater temporal precision in Y-type cells.

2.2. Psychophysics

Across stimulus parameters, the time constant that maximized motion encoding in cat (above) approximated values reported from primate retina [14], indicating that temporal fidelity may generalize across higher mammals, including humans. If the optimal time constant for temporal integration reflects the time scale at which retinal spike trains represent motion information, then presenting motion stimuli at shorter time scales should impair cortical motion processing. Impaired cortical motion processing, in turn, should impair psychophysical performance in a motion discrimination task. To test this, we next measured how human motion discrimination depends on stimulus duration, and compared the minimum exposure duration required for resolving motion direction at the perceptual level with the optimal integration times computed from the output of the retina and LGN.

Duration thresholds [25] were measured for a direction discrimination task in which observers discriminated motion (left vs. right) of a foveal Gabor stimulus. Stimulus size (0.33 deg at 2σ of the spatial Gaussian envelope) approximated foveal V1 receptive field size (0.25 deg; [26], small enough to avoid contrast dependent center-surround interactions reported for larger moving stimuli [27]. Spatial frequency was optimized for the human fovea (3.0 c/deg; [28]. Contrast and temporal frequency - parameters known to affect motion perception (e.g., [29-33] were systematically varied.

Psychophysical duration thresholds were very short, ranging from 5.6 ms at the highest temporal frequency tested (32 Hz) to about 65 ms at 0.5 Hz. Across stimuli, duration thresholds closely matched the optimal integration times computed from the responses of retinal X, Y and LGN cells (Figure 5A-D). Optimal integration times computed from the electrophysiological data and human duration thresholds both showed a robust dependence on temporal frequency that was largely independent of stimulus contrast. Thresholds increased dramatically at combinations of low contrast (< ~10%) and high temporal frequency (16 – 32 Hz). Because contrast sensitivity is known to decline strongly at high temporal frequencies [34] these increased thresholds likely reflect impaired stimulus detection. To examine the correspondence between the psychophysical and physiological results, we calculated asymptotic values of duration thresholds and τ_{opt} estimates at each temporal frequency (Figure 6). Asymptotic duration thresholds and τ_{opt} estimates for different cell types were closely correlated (human vs. retinal X, r = 0.99; human vs. retinal Y r =0.98; human vs. LGN X, r = 0.99; all $p < 0.0001$; Figure 7). Thus, duration thresholds and optimal integration times show the same quantitative dependence on temporal frequency.

Finally, it is important to highlight that the observed dependency on temporal frequency cannot be explained by the time it takes stimuli to cover a fixed proportion of its temporal cycle. This, arguably less interesting explanation, would lead to proportionally shorter thresholds with increasing temporal frequency. This was not the case. Expressed as a fraction of the stimulus cycle, human duration thresholds range from 1/5 of a cycle (4 arcmin) at 32 Hz to as little as 1/30 of a cycle (~ 0.7 arcmin) at 0.5Hz. This six-fold increase in the threshold displacement rules out the hypothesis that threshold requires a fixed displacement of the stimulus cycle. Analogously, if optimal integration times simply reflect the linear interaction between the sine wave stimulus and the low pass filter of the detector model, we should expect a slope of 1 / frequency (Figure 6A, dotted line). For all curves, the slope is significantly shallower (paired t-test; retinal X: $p < 0.01$; retinal Y: $p = 0.087$; LGN X: $p = 0.016$; human: $p < 0.01$) indicating that a proportionally smaller stimulus period is required for direction discrimination at higher temporal frequencies. Thus, the relationship between temporal frequency and both duration thresholds and τ_{opt} is non-linear. A likely

explanation is that at high temporal frequencies, temporal deviations in spike timing and unreliable spike generation – where a cell may skip its spike response to a stimulus period – become predominant in the response's temporal structure, and disproportionately increase the optimal integration time compared with lower temporal frequencies.

3. Discussion

For a range of stimulus parameters, we measured (1) the time scale at which a motion detector model optimally detects motion from retinal ganglion cell responses and (2) the temporal threshold of human motion perception. The time scales of motion encoding that we computed for cat closely match reported values obtained from macaque retina, *in vitro* [14]. We found that across conditions, both the physiological optimal integration time and the psychophysical temporal limit changed by more than 20-fold. This change was non-linear with changes in temporal frequency and contrast. Importantly, over the entire range of stimulus parameters, the two measurements were comparable: human duration thresholds and optimal integration times showed a corresponding dependency on temporal frequency and contrast (Figures 5, 6).

This pattern of results is consistent with the hypothesis that spike timing variability, which affects the optimal integration time, is an important factor limiting the temporal resolution of motion processing. Our interpretation is that spike timing variability sets the shortest sequence of spikes that needs to be analyzed by a motion detector to reliably signal motion, and that this temporal integration limits the minimum stimulus exposure required for an observer to perceive motion direction. Note that the brief integration times reported here are categorically different from the considerably longer temporal summation of motion signal investigated elsewhere (e.g., Burr, 1981), which is thought to primarily reflect integration of neural signals at stages downstream from motion detection. Our results show that the temporal limits of human motion perception closely adhere to the time scale at which motion information is best extracted from neuronal responses at the level of the retina and LGN, suggesting the high temporal fidelity of the retinal input is maintained and utilized in visual cortex.

3.1. Comparison to other reports of motion acuity

Our lowest threshold (5.6 ms at 32 Hz) is comparable to the shortest temporal order judgments reported in the literature, 3 – 6 ms [2-4]. It should be noted, however, that the stimuli used in previous studies demonstrating hyperacuity for temporal order judgments were lines or circles, sequentially flashed at two spatially separate locations. In each of these studies, total stimulus duration exceeded 10 ms. Our results show that even briefer presentations suffice: drifting Gabor stimuli that are narrowband in both space and time give similar temporal hyperacuity. Interestingly, psychophysical reports of temporal hyperacuity in vision are generally restricted to stimuli with motion cues. When such cues are removed, temporal acuity worsens to about 20-30ms [35, 36], which is comparable to the general temporal resolution of human vision [37]. This suggests that the motion system has access to temporal fidelity that ius not available to other visual sub-modalities.

The brief psychophysical thresholds measured here and in earlier studies (less than 10 ms) imply that motion direction can be computed from just a few spikes per cell. To illustrate this, Figure 7 shows side-by-side the 16 Hz stimulus successfully discriminated by human observers (7.9 ms threshold; Figure 6) and a retinal X cell's response to one period of a drifting sine wave. A cell typically fired 3 to 4 spikes during the time approximating the psychophysical stimulus presentation. For 32 Hz motion, which yielded the 5.6 ms psychophysical threshold, the number of spikes is even smaller. This suggests that for optimal stimuli, motion direction can be computed from just a few spikes per retinal input. Such estimates, of course, are likely to be noisy but can be improved by integrating responses from additional neurons [14]. This would establish a trade-off between temporal acuity and spatial acuity.

3.2. Comparing electrophysiology to psychophysics

This study connects results derived from neurophysiological recordings in an *in vivo* animal model with human psychophysical data – a link that should be treated with care [38]. To do so, it is important to consider the underlying assumptions along with the experimental choices that were made, to determine the extent to which the comparison of neurophysiological and psychophysical results was justified and meaningful.

First, we consider the assumptions behind neurophysiological recordings and accompanying modeling. The relevance of these results depends on (1) the functional significance of the optimal integration times, (2) the implications of mimicking pairs of cells with two responses from the same cell, and (3) the homology of temporal limits in motion processing between cat and primates including humans.

3.3. Significance of the optimal integration time

Our model analysis of ganglion cell spike trains yields brief optimal integration times, and earlier work showed feasibility of decoding spike trains on a similarly short time scale [13]. However, it not guaranteed that the time scale over which the motion system integrates its inputs is, in fact, optimized for temporal resolution. Indeed, a shorter-than-optimal integration time could result in attenuated, but nonetheless significant detection (Figure 4), establishing a trade-off between signal-to-noise ratio, i.e. 'certainty', and temporal resolution. Indeed, motion cortex may sacrifice signal-to-noise ratio to increase temporal resolution: for example, longer, sub-optimal temporal integration could compensate for an apparent loss of temporal resolution at the LGN X cell relay (Figure 6). Thus, while, τ_{opt} represents the time scale that would enable a cell to maximize signal-to-noise ratio of the motion-evoked response, the actual parameters used in cortical motion computation remain unclear – although our psychophysical results indicate they may be similar. Finally, whether the time scale for encoding motion within a given neural circuit is fixed or whether the same circuit can adapt its integration time depending on the task demands remains to be determined.

3.4. Use of single cells to model motion detector inputs

Spike train analysis was based on a common motion detector model, the bi-local correlator [39-41]. Essential to this, and most other motion-detection models, is the pair-wise correlation of signals from spatially separate receptive fields after one input channel is delayed, typically through low-pass filtering (Figure 2A). Here, we mimicked this mechanism by using two responses from the same cell, evoked by repeated presentations of the same visual stimulus. This assumes that ganglion cells of the same type share the same spatio-temporal response characteristics – an assumption that is supported by our experimental results and those reported elsewhere [42, 43]. The benefit of using two responses from the same cell is that this obviated the need to explicitly model a spatial separation and delay. Since the separation-delay combination would be different for detectors tuned to different stimulus temporal frequencies (speeds), this reduced the number of free parameters and simplified the model.

Hypothetical differences in the response characteristics of the cells that provide the correlator's inputs necessarily decrease the temporal correlation and, therefore, would require a longer integration time to reach the same correlation coefficient. Because the response characteristics of cells in our model are identical, the model gives an upper bound to the correlation coefficient and optimal integration time. With increasingly dissimilar cells, this upper bound could still be approximated by pooling over a larger number of inputs, and indeed, in macaque increasing the number of cells used in the computation of motion gives a better overall performance [14].

Finally, our use of repeated responses from single cells assumes that ganglion cells have independent noise, which is supported in the literature [44, 45]. While nearby retinal ganglion cells tend to fire correlated spikes [46, 47], correlated neural activity only has a weak effect on the encoding of motion speed [14]. Together, these arguments should permit the use of single neuron recordings to approximate motion encoding by two of more retinal inputs.

3.5. Species differences

We compared our results with those of Chichilnisky and Kalmar (2003), who employed an almost identical bi-local detector model to compute optimal time scales for motion discrimination from ganglion cell responses recorded in the macaque retina *in vitro*. For comparable stimuli, our estimates of optimal integration times from cat X and Y-cells closely match the equivalent 'optimal temporal filter widths' reported for macaque parasol cells [13]. The optimal integration time for a cat retinal ganglion cell responding to a sine wave drifting at 14 deg sec^{-1} is 12 ms. For macaque parasol cells responding to a bar also moving at 14 deg sec^{-1}, the optimal time scale reported by Chichilnisky and Kalmar (2003) is 13 ms. This suggests that in terms of the time scale of motion encoding, cat X and Y and macaque parasol cells are comparable.

The similarity between response temporal fidelity in cat and primate retina is perhaps not surprising because variability in spike rate and spike timing is likely to be similar across these species. Response variability at the level of the retina variability depends on four key factors: neural noise, contrast sensitivity, refractory period, and peak firing rate. Because these are fundamental properties shared among equivalent cell types (e.g., cat Y and primate parasol), one would not expect major differences between them, and none have been reported. On the contrary, for a spatio-temporal white noise stimulus, cat and macaque retinal responses appear to be highly similar (cat: [48-50]; macaque: [21, 42]. Thus, our measurements agree with the established similarities of cat ganglion cell and macaque parasol cell responses. Because parasol cells are thought to underlie motion vision in macaques and humans, the observed similarity also suggests that measurements of responses in the front-end visual system in both cat and macaque can make valid predictions for motion vision in humans.

3.6. Psychophysical assumptions

Finally, we considered the factors affecting psychophysical estimates of temporal limits in motion perception. The results presented here are conditional on the definition of the stimulus duration and the psychometric threshold. Moving stimuli were shown in a Gaussian temporal envelope, whose duration is, in theory, infinite. In practice, duration is typically defined as 2σ of the temporal Gaussian (cf. [28], which includes 68% of total stimulus contrast. Detection threshold was conservatively defined as 82% correct, a commonly used optimal choice for a QUEST staircase [51]. Although our definition of the stimulus duration and selection of the threshold level follow established conventions, they are arbitrary. When tested, the use of other conventions resulted in small changes in duration threshold that did not affect our main findings.

Psychophysical threshold can be affected by inadvertent slips of the subject's attention, especially for very brief stimuli. To prevent this, the delay between button press and stimulus onset was fixed and therefore predictable for the subjects, who were experienced at the psychophysical task. The use of adaptable staircases to measure thresholds further minimized any possible effects of inattention. The remaining factors influencing psychophysical results are the task and the stimulus parameters. Here, the task was the simplest possible discrimination task. Stimulus parameters were optimized for human motion perception [28] and were designed to avoid known inhibitory effects of large moving stimuli [25].

Without direct physiological measurements of the neural correlate of the motion detector's integrator, we can only infer the exact quantitative relationship between the temporal fidelity of the retina's output and the temporal limits of motion vision. Instead, we report here for closely matched stimulus conditions, strong similarity and co-dependency on stimulus parameters between predicted optimal integration times and human duration thresholds. Our findings support the hypothesis that the temporal limits of motion vision approximate the limits set by motion encoding in the retina.

4. Methods

4.1. Electrophysiological preparation and recordings

Extracellular single unit recordings from retinal ganglion cells and LGN cells were obtained with tungsten microelectrodes (TM33B20KT, World Precision Instruments, USA, typical impedance 2.0 MΩ at 1.0 kHz) from 19 anesthetized adult cats of either sex (3 - 5 kg). Surgical procedures were standard and in accordance with the guidelines of the Law on Animal Research of the Netherlands and of the Utrecht University's Animal Care and Use Committee.

Anesthesia was induced by ketamine hydrochloride injection (Aescoket-plus, 20 mg kg^{-1}, i.m.). Following preparatory surgery, anesthesia was maintained by artificial ventilation with a mixture of 70% N_2O - 30% O_2 and halothane (Halothaan, 0.4 - 0.7%). To minimize eye movements, muscle paralysis was induced and maintained throughout the experiment by infusion of pancuronium bromide (Pavulon, 0.1 mg kg^{-1} hr^{-1}, i.v.). Oxygen-permeable contact lenses (+3.5 to +5 diopters, courtesy of NKL, Emmen, The Netherlands) were used to both focus the visual stimulus on the retina and protect the corneae.

LGN and optic tract recordings were obtained at approximately 10 and 20 mm below the cortical surface at Horsley-Clarke coordinates A8, L10 [52]. Action potentials from single cells were detected with a window discriminator (BAK Electronics Inc.) and digitized at 2.0kHz (PCI 1200, National Instruments) for on-line analysis and storage (Apple Macintosh G4 computer, custom-written software).

4.2. Visual stimulation

Stimuli for electrophysiology experiments were computer-generated (ATI rage graphics card, Macintosh G4 computer, custom-written software), presented on a linearized 19", 100 Hz CRT monitor (Sony Trinitron Multiscan 400PS) at 57 cm from the optic node and centered on the receptive field of the cell under study. Mean luminance was 54 $cd \cdot m^{-2}$. For those cells (<15%) that showed significant response modulation to the 100Hz refresh rate of the monitor [53], the frame rate was increased to 120Hz.

For each cell, spatial and temporal tuning curves were measured using drifting sinusoidal gratings (spatial frequency 0.1 - 4.0 cycles deg^{-1}, temporal frequency 0.5 – 50 Hz). Cells were classified as X or Y on the basis of a null-test [54]. Responses to twenty repeats of a 3 second presentation of drifting sine wave gratings were used for the model analysis. Sinusoidal gratings fully covered the receptive field and spatial frequency was optimized for each cell (average 0.8 cycles deg^{-1}). Temporal frequency and luminance contrast were varied (0.5 – 16 Hz and from 10 - 70% Michelson contrast, respectively). A stimulus block consisted of 6 temporal frequencies and 7 contrasts, resulting in 42 stimuli presented in a random order. Data presented in this study were obtained from cells with receptive fields located within the central 15 degrees of the visual field. Only single unit recordings that were stable during at least 20 repeats of the stimulus block and showed significant response modulation to the high contrast stimuli were accepted for analysis.

4.3. Psychophysics

Stimuli for human psychophysics experiments were computer-generated using Matlab (The Mathworks; Natick, MA), the Psychophysics Toolbox [55] and Video Toolbox [56], and shown on a linearized monitor (800 x 600 pixels, 200 Hz). We used a bit stealing technique [57] to expand gray-scale resolution from 256 to 768 levels. To obtain a 200 Hz refresh rate, we used a high-speed PROCALIX monitor (Totoku, Irving, TX) driven by a MP960 graphics card (VillageTronic, Berlin, Germany). Viewing was binocular at 83 cm (yielding 2 x 2 arcmin per pixel). Luminance of the gray screen background was 41.1 cd/m^2. Three observers participated in the experiment (first and second authors and a naïve observer). All procedures complied with institutionally reviewed guidelines for human subjects and all subjects provided written informed content.

Stimuli were vertically oriented Gabor patches, comprising a drifting vertical sine grating windowed by a stationary two-dimensional Gaussian envelope (2σ width = 20 arcmin, spatial frequency = 3 cycles/deg, starting phase randomized). Gabor contrast was modulated by a temporal Gaussian envelope. Peak Gabor contrast and temporal frequency were varied in a 7 x 5 design (0.5 – 32 Hz and 5 – 80 %, respectively). The observers' task was to discriminate motion (left vs. right) of a briefly presented Gabor

patch. Duration thresholds [25, 58, 59] were estimated using two interleaved QUEST staircases [51], where staircases adjusted the standard deviation of the temporal Gaussian envelope and converged to 82% correct. Duration was defined as 2σ width of the Gaussian envelope. The entire set of 35 conditions was repeated four times in random order. This yielded eight threshold estimates per condition, of which the first two thresholds discarded as practice. Trials were self-paced. Each trial began with a key-press, followed by a stimulus 350 ms later. Feedback was provided.

Given that we were expecting very brief motion direction thresholds (especially for high temporal frequency conditions), we paid close attention to what is the lower limit of temporal stimulus duration that we can accurately present and measure. Stimuli were displayed on a 200 Hz monitor by discrete sampling of the temporal Gaussian waveform every 5 ms, while ensuring that the middle sample always contained the peak of the Gaussian [59]. For example, a Gabor patch presented in a temporal Gaussian window with $2\sigma = 5.6$ ms (our lowest threshold: 32 Hz motion, 80% peak contrast) would be shown in 3 video frames displaying 20.1, 100, and 20.1% of the peak contrast (see Figure 7 for another example). To test for possible floor effects at the highest stimulus temporal frequency (32 Hz) we measured duration thresholds for 8, 16, and 32 Hz motion at 100 Hz and 200 Hz frame rates. Substantially lower thresholds for 8 and 16 Hz stimulus presented at 200 Hz would indicate deleterious under-sampling of the Gaussian waveform at 100 Hz. Respective thresholds for 8 and 16 Hz motion were 7.9% and 8.3% lower at 200 Hz than at 100 Hz frame rate, likely indicating the effects of higher fidelity motion representation at 200Hz. In contrast, the threshold for 32 Hz motion was 28% lower at 200 Hz, indicating a floor effect for 32 Hz motion at 100 Hz frame rate. Based on these measurements, we can assert that our set up is adequate for measuring the 32 Hz stimulus presented at a frame rate of 200 Hz.

4.4. Model analysis

Essential to most motion detection models is the integration of visual signals from spatially separated receptive fields [39, 40]. Known as a bi-local motion detector (Figure 2A), the model's output reflects the time-varying correlation between the input signals, one of which is temporally delayed relative to the other (Hassenstein and Reichardt, 1956). The delay causes sensitivity to the temporal sequence of stimulation of the two receptive fields, and combined with a threshold nonlinearity renders its response selective for motion direction. Because detector function is based on temporal correlations, motion detection depends on temporal similarity of the input signals.

The input signals in our model are retinal spike trains. Their temporal correlation is determined by the magnitude of noise variations (variability) in these spike patterns. If variability in the spike pattern is large then the correlation between responses from the two cells will be small. Thus, variability in the cells' temporal spike pattern should limit motion detection. The correlator can counter this variability, by integrating the spike trains over a finite time window to increase temporal overlap. But temporal integration comes at a cost of increasing the time scale at which motion may be resolved. To assess this trade-off, we measured for the recorded ganglion cell responses how the integration time that optimizes correlation detection varies with stimulus contrast and temporal frequency – parameters expected to affect ganglion cell spike response variability.

The bi-local detector was modeled as a correlator unit whose two inputs signals were pairwise combinations of spike trains recorded from a single ganglion cell, evoked by repeated presentation of the same visual stimulus (minimum of 20 stimulus repeats; n = 33 retinal X cells, 4 retinal Y cells, and 20 LGN X cells). Using responses on alternate trials obtained from a single cell simplifies the model, as it obviates explicit modeling of spatial separation and time delay of the two input receptive fields, and maximizes temporal correlations independent of temporal frequency. As such, the model represents a detector whose input signals are spike responses from two cells with identical response characteristics and spatio-temporal receptive fields, but subject to independent noise variations [44, 45]. Differences in response characteristics and receptive fields between cells necessarily decrease temporal similarity of their spike responses – resulting in poorer detection performance. Therefore, our model provides an upper limit to motion detector performance given a ganglion cell's spike response variability.

Input to the model was a set of recorded spike trains $s_i(t)$, $n \geq 20$,

$$(1)\ s_i(t) = \sum_{\{t_j\}} \delta(t - t_j);\ i = 1,,,n.$$

Spike trains were passed through a first order filter with time constant τ, and normalized for τ, adding an exponential tail with an integral of 1 to each spike,

$$(2)\ x_i(t,\tau) = s_i(t) * \frac{e^{-1/\tau}}{\tau}$$

From this set, pairs of spike trains were multiplied, integrated and normalized to the integral of the first spike train,

$$(3)\ y(\tau) = \frac{2 \cdot \sum_{k=1}^{n} \sum_{m=k+1}^{n} \int_0^T dt \cdot x_k(t,\tau) \cdot x_m(t,\tau)}{(n-1) \sum_{k=1}^{n} \int_0^T dt \cdot x_k(t,\tau)^2}$$

This operation was performed for a series of τ ranging from 1 - 500 ms resulting in $y(\tau)$. Spike trains $s_i(t)$ were then shuffled by redistributing the inter-spike intervals in each spike train. This yields spike trains $s_i'(t)$ that have identical mean firing rates, yet lack all stimulus related temporal structure. Repeated for shuffled spike trains $s_i'(t)$, the same procedure results in $y'(\tau)$, which was used as a measure of chance-level coincidence between spikes in the two the spike trains given the mean spike rate. The difference function $C(\tau)$ describes the specific contribution of the temporal structure of the input spike trains to the coincidence detected by the hypothetical correlator unit.

$$(4)\ C(\tau) = y(\tau) - y'(\tau)$$

This simple motion model incorporates low-pass filtering (temporal integration) and correlation of input signals — two essential components of established models of motion perception [39, 40, 60]. For each cell and stimulus condition, all possible response pairs (180 minimum) were used in the simulations. τ_{opt} was calculated by averaging the results from each spike train pair. Note that the actual procedure followed was the closest possible numerical approximation (time base 0.5 ms) to the equations presented here.

Acknowledgments: We thank Davis Glasser for help with manuscript preparation.

Author contributions: Conceptualization, B.G.B., D.T., M.J.M.L., J.S.L., and W.A.G.; Methodology, B.G.B., D.T., and M.J.M.L.; Software, B.G.B., D.T., and M.J.M.L.; Validation, B.G.B., D.T., M.J.M.L., J.S.L., and W.A.G.; Formal Analysis, B.G.B. and D.T.; Investigation, B.G.B. and D.T.; Data Curation, B.G.B. and D.T.; Resources, M.J.M.L., J.S.L., and W.A.G.; Writing—Original Draft Preparation, B.G.B. and D.T.; Writing—Review & Editing, B.G.B., D.T., M.J.M.L., J.S.L., and W.A.G.; Visualization, B.G.B. and D.T.; Supervision, M.J.M.L., J.S.L., and W.A.G.; Project Administration, J.S.L., and W.A.G.; Funding Acquisition, M.J.M.L., J.S.L., and W.A.G.

Funding: This research was funded by NWO/ALW grant 805.04.134 (B.G.B, M.J.M.L.) and National Institutes of Health grants EY028188 (B.G.B.).

Conflicts of Interest: The authors declare no conflict of interest.

References

1. Exner, S., *Experimentelle Untersuchung der einfachsten psychischenProcesse: III. Abhandlung, Der persönlichen Gleithung zweiter Teil.* Pflügers Archiv für die gesamte Physiologie der Menschen und der Thiere, 1875. **11**: p. 403-432.
2. Sweet, A.L., *Temporal discrimination by the human eye.* American Journal of Psychology, 1953. **66**: p. 185–198.
3. Wehrhahn, C. and D. Rapf, *ON- and OFF-pathways form separate neural substrates for motion perception: psychophysical evidence.* J Neurosci, 1992. **12**(6): p. 2247-2250.
4. Westheimer, G. and S.P. McKee, *Perception of temporal order in adjacent visual stimuli.* Vision Res, 1977. **17**(8): p. 887-92.
5. Born, R.T. and D.C. Bradley, *Structure and function of visual area MT.* Annu Rev Neurosci, 2005. **28**: p. 157-189.
6. Schmolesky, M.T., et al., *Signal timing across the macaque visual system.* Child Abuse & Neglect, 1998. **22**(6): p. 481-91.
7. Fairbank, B.A., Jr., *Moving and nonmoving visual stimuli: a reaction time study.* Percept Mot Skills, 1969. **29**(1): p. 79-82.
8. Buracas, G.T., et al., *Efficient discrimination of temporal patterns by motion-sensitive neurons in primate visual cortex.* Neuron, 1998. **20**(5): p. 959-69.
9. Elstrott, J. and M.B. Feller, *Vision and the establishment of direction-selectivity: a tale of two circuits.* Curr Opin Neurobiol, 2009. **19**(3): p. 293-7.
10. Lochmann, T., T.J. Blanche, and D.A. Butts, *Construction of direction selectivity through local energy computations in primary visual cortex.* PLoS One, 2013. **8**(3): p. e58666.
11. Peterson, M.R., B. Li, and R.D. Freeman, *The derivation of direction selectivity in the striate cortex.* J Neurosci, 2004. **24**(14): p. 3583-91.
12. Stanley, G.B., et al., *Visual orientation and directional selectivity through thalamic synchrony.* J Neurosci, 2012. **32**(26): p. 9073-88.
13. Chichilnisky, E.J. and R.S. Kalmar, *Temporal resolution of ensemble visual motion signals in primate retina.* J Neurosci, 2003. **23**: p. 6681-6689.
14. Frechette, E.S., et al., *Fidelity of the ensemble code for visual motion in primate retina.* J Neurophysiol, 2005. **94**: p. 119-135.
15. Borghuis, B.G., *Spike timing precision in the visual front-end*. 2003, Utrecht: Utrecht University Library. 97-121.
16. Butts, D.A., et al., *Temporal precision in the neural code and the timescales of natural vision.* Nature, 2007. **449**(7158): p. 92-5.
17. Angueyra, J.M. and F. Rieke, *Origin and effect of phototransduction noise in primate cone photoreceptors.* Nat Neurosci, 2013. **16**(11): p. 1692-700.
18. Mainen, Z.F. and T.J. Sejnowski, *Reliability of spike timing in neocortical neurons.* Science, 1995. **268**: p. 1503-1506.
19. Reid, R.C., J.D. Victor, and R.M. Shapley, *The use of m-sequences in the analysis of visual neurons: linear receptive field properties.* Vis. Neurosci., 1997. **14**(6): p. 1015-27.
20. Reinagel, P., *Information theory in the brain.* Curr Biol, 2000. **10**: p. R542-R544.
21. Uzzell, V.J. and E.J. Chichilnisky, *Precision of spike trains in primate retinal ganglion cells.* J Neurophysiol, 2004. **92**(2): p. 780-9.
22. Hass, C.A., et al., *Chromatic detection from cone photoreceptors to V1 neurons to behavior in rhesus monkeys.* J Vis, 2015. **15**(15): p. 1.
23. Beaman, C.B., S.L. Eagleman, and V. Dragoi, *Sensory coding accuracy and perceptual performance are improved during the desynchronized cortical state.* Nat Commun, 2017. **8**(1): p. 1308.
24. van Rossum, M.C., *A novel spike distance.* Neural. Comput., 2001. **13**(4): p. 751-63.

25. Tadin, D., et al., *Perceptual consequences of center-surround antagonism in visual motion processing.* Nature, 2003. **424**: p. 312-315.
26. Dow, B.M., et al., *Magnification factor and receptive field size in foveal striate cortex of the monkey.* Exp. Brain Res., 1981. **44**(2): p. 213-28.
27. Tadin, D., *Suppressive mechanisms in visual motion processing: From perception to intelligence.* Vision Res, 2015. **115**(Pt A): p. 58-70.
28. Watson, A.B. and K. Turano, *The optimal motion stimulus.* Vision Res., 1995. **35**(3): p. 325-36.
29. Burr, D.C., *Temporal summation of moving images by the human visual system.* Proc. R. Soc. Lond. B Biol. Sci., 1981. **211**(1184): p. 321-39.
30. Burr, D.C. and B. Corsale, *Dependency of reaction times to motion onset on luminance and chromatic contrast.* Vision Res., 2001. **41**(8): p. 1039-48.
31. Edwards, M., D.R. Badcock, and S. Nishida, *Contrast sensitivity of the motion system.* Vision Res., 1996. **36**(16): p. 2411-21.
32. Nakayama, K. and G.H. Silverman, *Detection and discrimination of sinusoidal grating displacements.* J. Opt. Soc. Am. A, 1985. **2**(2): p. 267-74.
33. van de Grind, W.A., J.J. Koenderink, and A.J. van Doorn, *Influence of contrast on foveal and peripheral detection of coherent motion in moving random-dot patterns.* J. Opt. Soc. Am. A, 1987. **4**(8): p. 1643-52.
34. Burr, D.C. and J. Ross, *Contrast sensitivity at high velocities.* Vision Res, 1982. **22**(4): p. 479-84.
35. Tadin, D., et al., *High temporal precision for perceiving event offsets.* Vision Res, 2010. **50**(19): p. 1966-71.
36. Zanker, J.M. and J.P. Harris, *On temporal hyperacuity in the human visual system.* Vision Res, 2002. **42**(22): p. 2499-508.
37. Kelly, D.H., *Adaptation effects on spatio-temporal sine-wave thresholds.* Vision Res, 1972. **12**(1): p. 89-101.
38. Teller, D.Y., *Linking propositions.* Vision Res, 1984. **24**(10): p. 1233-46.
39. Barlow, H.B. and W.R. Levick, *The mechanism of directionally selective units in rabbit's retina.* J Physiol, 1965. **178**(3): p. 477-504.
40. Hassenstein, B. and W. Reichardt, *Systemtheoretische Analyse der Zeit-, Reihenfolgen- und Vorzeichenauswertung bei der Bewegungsperzeption des Russelkäfers Chlorophanus.* Z. Naturforsch., 1956. **11b**: p. 513-525.
41. Reichardt, W., *Autocorrelation, a principle for the evaluation of sensory information by the central nervous system*, in *Sensory Communication*, W.A. Rosenblith, Editor. 1961, MIT Press: Cambridge, MA. p. 303-317.
42. Chichilnisky, E.J. and R.S. Kalmar, *Functional asymmetries in ON and OFF ganglion cells of primate retina.* J Neurosci, 2002. **22**(7): p. 2737-47.
43. Reinagel, P. and R.C. Reid, *Precise firing events are conserved across neurons.* J Neurosci, 2002. **22**(16): p. 6837-41.
44. Croner, L.J., K. Purpura, and E. Kaplan, *Response variability in retinal ganglion cells of primates.* Proc Natl Acad Sci U S A, 1993. **90**: p. 8128-8130.
45. Ginsburg, K.S., J.A. Johnsen, and M.W. Levine, *Common noise in the firing of neighbouring ganglion cells in goldfish retina.* J Physiol, 1984. **351**: p. 433-450.
46. Mastronarde, D.N., *Correlated firing of cat retinal ganglion cells. II. Responses of X- and Y-cells to single quantal events.* J Neurophysiol, 1983. **49**(2): p. 325-49.
47. Mastronarde, D.N., *Interactions between ganglion cells in cat retina.* J Neurophysiol, 1983. **49**(2): p. 350-65.
48. Dan, Y., J.J. Atick, and R.C. Reid, *Efficient coding of natural scenes in the lateral geniculate nucleus: experimental test of a computational theory.* J Neurosci, 1996. **16**(10): p. 3351-62.
49. Keat, J., et al., *Predicting every spike: a model for the responses of visual neurons.* Neuron, 2001. **30**(3): p. 803-17.

50. Reich, D.S., et al., *Response variability and timing precision of neuronal spike trains in vivo.* J Neurophysiol, 1997. **77**: p. 2836-2841.
51. Watson, A.B. and D.G. Pelli, *QUEST: a Bayesian adaptive psychometric method.* Percept. Psychophys., 1983. **33**(2): p. 113-20.
52. Reinoso-Suarez, F., *Topographischer Hirnatlas der Katze.* Translated edition by E. Merck AG, Darmstad, Germany, 1961: p. T 24.
53. Eysel, U.T. and U. Burandt, *Fluorescent tube light evokes flicker responses in visual neurons.* Vision Res, 1984. **24**(9): p. 943-8.
54. Hochstein, S. and R.M. Shapley, *Quantitative analysis of retinal ganglion cell classifications.* J. Physiol., 1976. **262**(2): p. 237-64.
55. Brainard, D.H., *The Psychophysics Toolbox.* Spat. Vis., 1997. **10**(4): p. 433-6.
56. Pelli, D.G., *The VideoToolbox software for visual psychophysics: Transforming numbers into movies.* Spat. Vis., 1997. **10**: p. 437-442.
57. Tyler, C.W., *Colour bit-stealing to enhance the luminance resolution of digital displays on a single pixel basis.* Spat. Vis., 1997. **10**(4): p. 369-77.
58. Murray, S.O., et al., *Sex Differences in Visual Motion Processing.* Curr Biol, 2018. **28**(17): p. 2794-2799 e3.
59. Tadin, D., J.S. Lappin, and R. Blake, *Fine temporal properties of center-surround interactions in motion revealed by reverse correlation.* J Neurosci, 2006. **26**(10): p. 2614-22.
60. Adelson, E.H. and J.R. Bergen, *Spatiotemporal energy models for the perception of motion.* J. Opt. Soc. Am. A, 1985. **2**(2): p. 284-99.

Figure legends

Figure 1. Retinal ganglion cell responses to drifting sinusoidal grating stimuli. Raster plot of a 1 second section of the response of a single retinal ganglion cell to drifting sinusoidal grating stimuli, varying in contrast (10 - 70%) and temporal frequency (left 2.0; right 8.0 Hz). Each dot in the display represents a spike. Each line represents the response to a single presentation of the stimulus. Stimuli were presented randomly interleaved, and repeated a minimum of 20 times.

Figure 2. Temporal integration improves correlation detection. (A) Bilocal motion detector model. Correlator unit X receives input from two units sampling the retinal image with spatially separated receptive fields, RF1 and RF2. Through cross-multiplication of the input spike trains, the correlator's output is high only when it receives positive input synchronously. The combination of spatial separation Δx and temporal delay Δt in one of the input channels tunes the detector to stimulus motion with a velocity of $\Delta x/\Delta t$. This elementary model captures the essence of spatio-temporal correlation of the retinal input, a requirement for any motion detection model. Because the correlator also responds to non-directional, uniform flicker, directional selectivity generally follows from a comparison of the output of two or more detectors, tuned to opposite motion directions. (B) A short integration time (2 ms) gives little overlap between input signals 1 (top) and 2 (middle). Only highly coincident spikes (temporal deviation < ~4 ms) result in non-zero output (bottom). (C) A long integration time (100 ms) gives substantial overlap between the two input signals and results in a strong output signal (bottom).

Figure 3. Computing the optimal integration time. From the difference between the correlation curve for the recorded (solid squares) and shuffled spike trains (open squares) we obtained a relative correlation curve (red circles; see Model for details). We defined the optimal integration time (τ_{opt}) as the time constant where the relative correlation curve peaks. At this integration time, the correlator best extracts motion information from the temporal structure of the input spike trains. Optimal integration times were computed in Matlab, following cubic spline interpolation of the 15 data points.

Figure 4. Stimulus parameters set optimal integration time for correlation detection. Relative correlation curves based on the data partially displayed in Figures 1 and 3. The optimal integration time (integration time at peak) decreases with increasing temporal frequency. Contrast (10 - 70%) determines total correlation (peak height), but above about 10% has little effect on the optimal integration time.

Figure 5. Optimal integrations time and duration thresholds decrease with increasing temporal frequency but change little with contrast. (A-C) Optimal integration times for all combinations of stimulus temporal frequency and contrast for 33 retinal X cells, 4 retinal Y cells, and 20 LGN X cells. Optimal integration time systematically decreased with increasing temporal frequency, but was largely independent of contrast above about 10%. Error bars show mean ± SEM. (D) Minimal presentation duration required for human observers to discriminate motion direction as a function of stimulus temporal frequency and contrast. Duration threshold decreased with temporal frequency of the sinewave grating. Above about 10%, duration threshold was largely independent of stimulus contrast. Error bars show mean ± SEM for four subjects.

Figure 6. Optimal integration time closely matches duration threshold across stimulus conditions. (A) Optimal integration times, averaged across responses to 40 - 70% contrast stimuli, decrease with increasing temporal frequency. A similar decrease is observed for human duration thresholds. The slope of each curve deviates systematically from 1/frequency (dotted line). Optimal integration time and duration threshold do not simply reflect detection of a fixed stimulus displacement. (B) Optimal integration times closely match duration thresholds, except at the highest temporal frequencies, where optimal integration times for retinal Y cells are shorter than the duration threshold, i.e., their temporal fidelity exceeds psychophysical performance.

666
667 **Figure 7. Direction discrimination apparently requires few spikes per cell.** Human observers were
668 asked to discriminate motion direction of a drifting sine wave grating (16 Hz) in a spatial Gaussian envelope
669 (Gabor patch, top left). (A) Contrast of the Gabor patch was Gaussian modulated in time. Presented at 200
670 Hz, this paradigm allowed very brief presentations of stimulus motion. Example shows the discrete sam-
671 pling of contrast values ($\sigma = 7.9$ ms, 70% contrast). (B) To a drifting sine wave (16 Hz) of equivalent spatial
672 frequency and same contrast, a cat retinal ganglion cell fires ~4 spikes.
673

674 Figure 1.
675

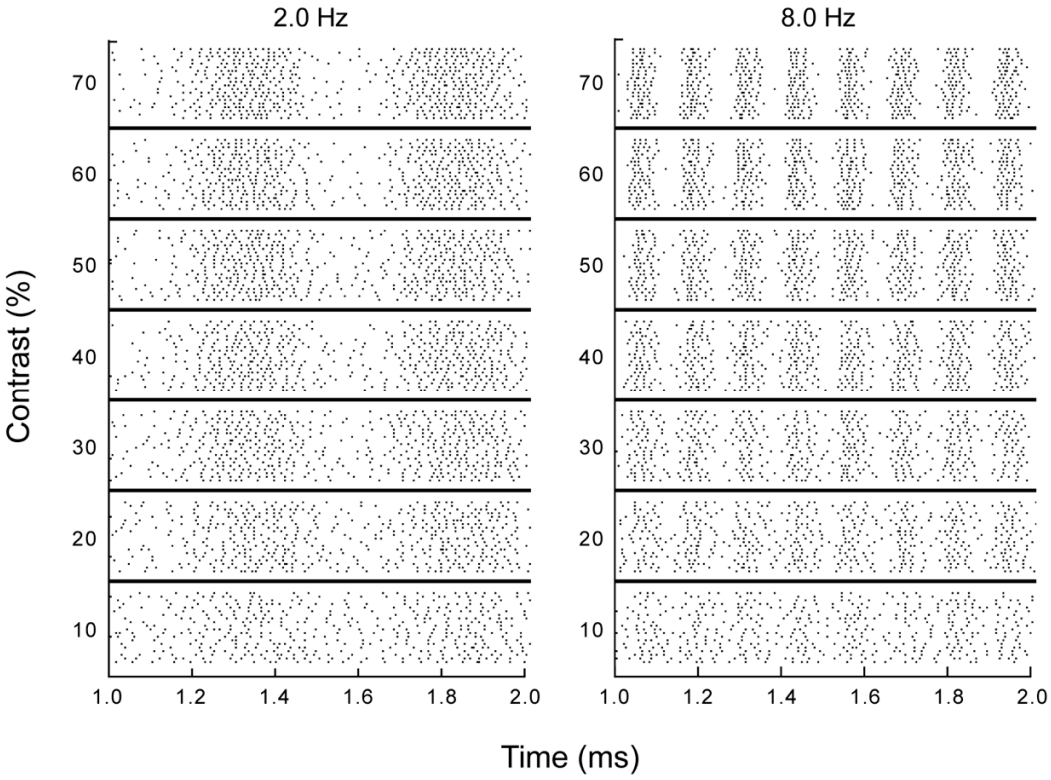

676
677

Figure 2.

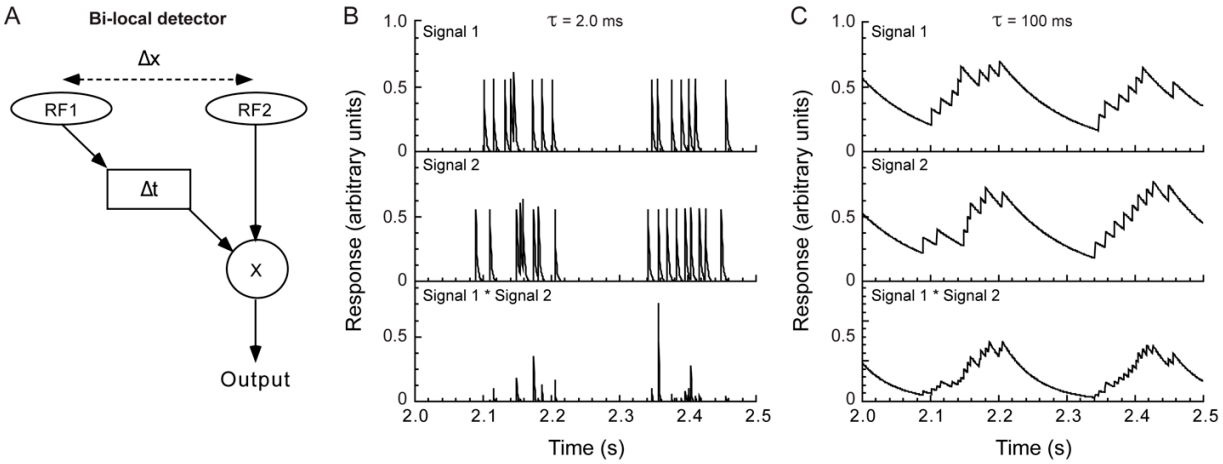

Figure 3.

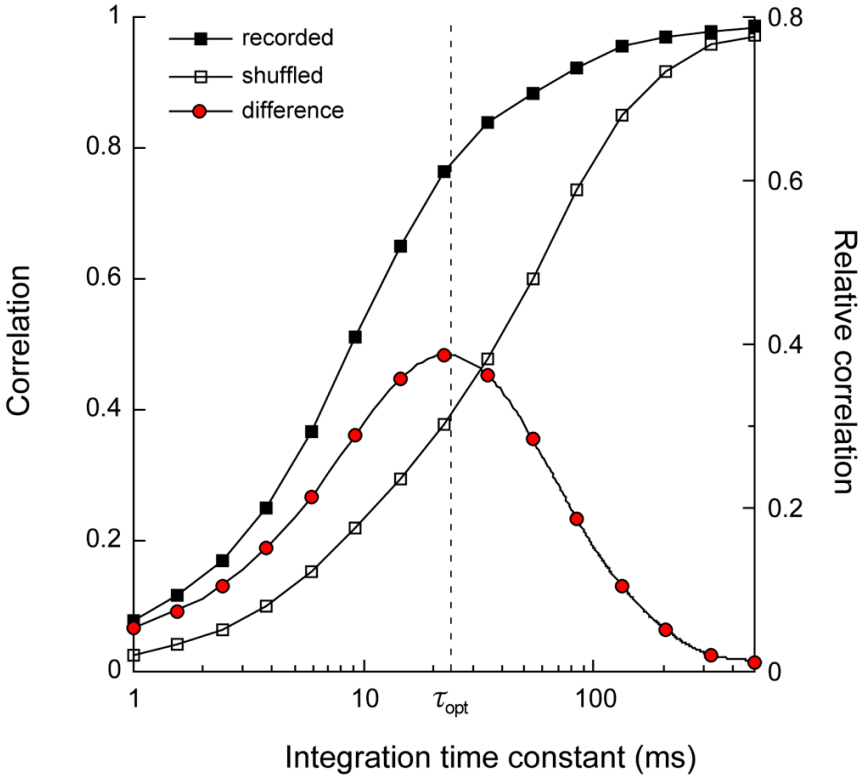

690 Figure 4.

691

692

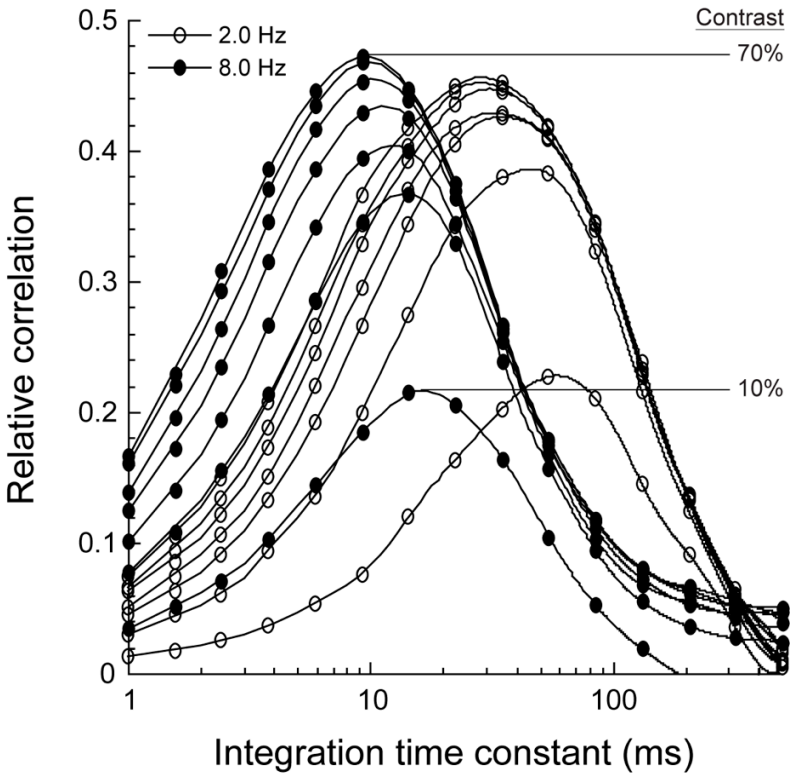

693

694

695

Figure 5.

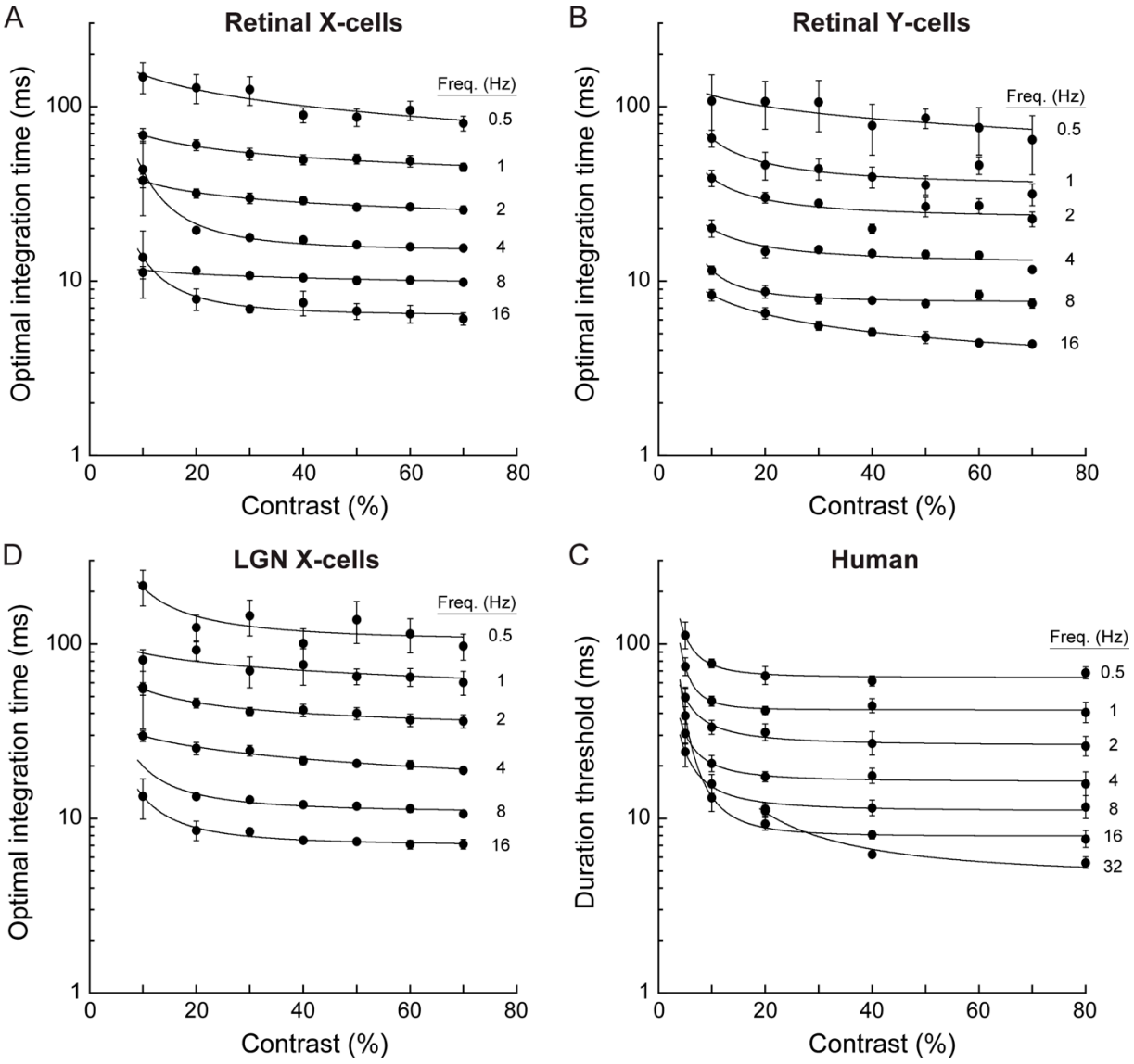

Figure 6.

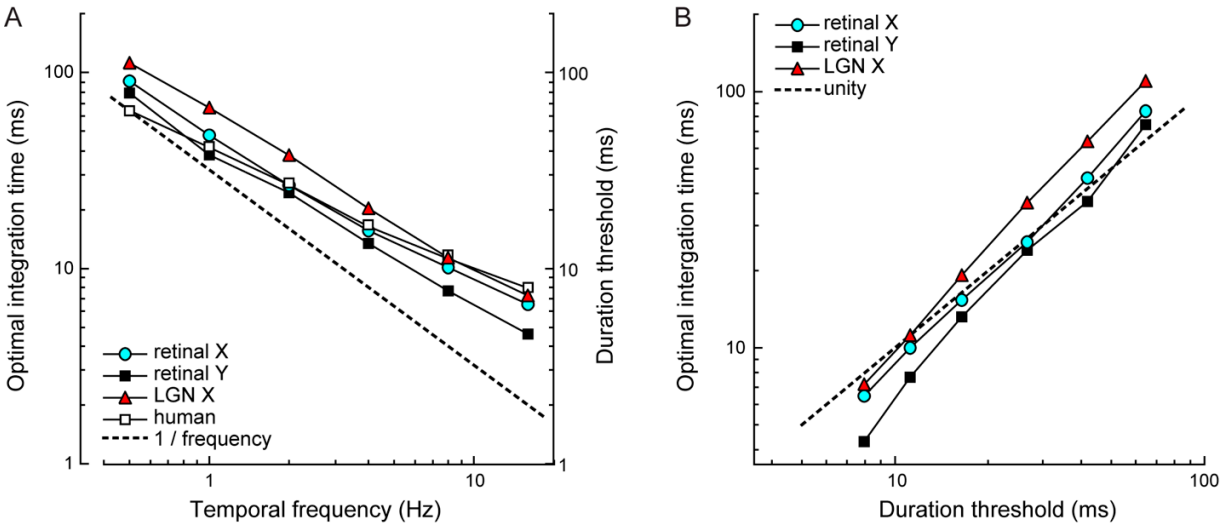

Figure 7.